01 Apr 2023

Molecular Cluster Complex of High-Valence Chromium Selenide Carbonyl as Effective Electrocatalyst for Water Oxidation

Ibrahim Munkaila Abdullahi

Manashi Nath
Missouri University of Science and Technology, nathm@mst.edu

Recommended Citation

I. M. Abdullahi and M. Nath, "Molecular Cluster Complex of High-Valence Chromium Selenide Carbonyl as Effective Electrocatalyst for Water Oxidation," *Catalysts*, vol. 13, no. 4, article no. 721, MDPI, Apr 2023. The definitive version is available at https://doi.org/10.3390/catal13040721

catalysts

MDPI

Article

Molecular Cluster Complex of High-Valence Chromium Selenide Carbonyl as Effective Electrocatalyst for Water Oxidation

Ibrahim Munkaila Abdullahi and Manashi Nath *

Department of Chemistry, Missouri University of Science and Technology, Rolla, MO 65409, USA
* Correspondence: nathm@mst.edu; Tel.: +1-(573)-341-7160

Abstract: Developing simple, affordable, and environmentally friendly water oxidation electrocatalysts with high intrinsic activity and low overpotential continues to be an area of intense research. In this article, a trichromium diselenide carbonyl cluster complex $(Et_4N)_2[Se_2Cr_3(CO)_{10}]$, with a unique bonding structure comprising bridging Se groups, has been identified as a promising electrocatalyst for oxygen evolution reaction (OER). This carbonyl cluster exhibits a promising overpotential of 310 mV and a low Tafel slope of 82.0 mV dec^{-1} at 10 $mAcm^{-2}$, with superior durability in an alkaline medium, for a prolonged period of continuous oxygen evolution. The mass activity and turnover frequency of 62.2 Ag^{-1} and 0.0174 s^{-1} was achieved, respectively at 0.390 V vs. RHE. The Cr-complex reported here shows distinctly different catalytic activity based on subtle changes in the ligand chemistry around the catalytically active Cr site. Such dependence further corroborates the critical influence of ligand coordination on the electron density distribution which further affects the electrochemical activation and catalytic efficiency of the active site. Specifically, even partial substitution with more electronegative substituents leads to the weakening of the catalytic efficiency. This report further demonstrates that metal carbonyl chalcogenides cluster-type materials which exhibit partially occupied sites and high valence in their metal sites can serve as catalytically active centers to catalyze OER exhibiting high intrinsic activity. The insight generated from this report can be directly extrapolated to 3-dimensional solids containing similar structural motifs, thereby aiding in optimal catalyst design.

Keywords: water splitting; molecular complex; carbonyl cluster; oxygen evolution reaction; chromium selenide

Citation: Abdullahi, I.M.; Nath, M. Molecular Cluster Complex of High-Valence Chromium Selenide Carbonyl as Effective Electrocatalyst for Water Oxidation. *Catalysts* **2023**, *13*, 721. https://doi.org/10.3390/catal13040721

Academic Editor: Vincenzo Baglio

Received: 6 March 2023
Revised: 4 April 2023
Accepted: 6 April 2023
Published: 11 April 2023

1. Introduction

The search for highly active and durable materials for sustainable energy conversion and storage has been attracting significant attention owing to the rapid depletion of fossil fuels amidst the growing concern about global warming. Water oxidation has been identified as an effective approach to generate clean hydrogen, which is one of the most sustainable zero carbon emission energy sources with a high energy density of 142 kJ kg^{-1} [1]. However, because of the sluggish kinetics of oxygen evolution reactions (OER) during water oxidation, electrocatalysts are generally employed to reduce the activation barrier along with stabilizing the OER intermediate adsorption on the catalyst surface [2–4]. Although significant research has led to the identification of precious metal-based oxides as efficient OER electrocatalysts, the high cost and scarcity of precious metals such as Ir, Ru, and Pt, severely limit their widespread practical applications. Over the last several years non-precious transition metal-based compositions have gained attention as OER electrocatalysts owing to their unprecedented high activity, tunable electrochemical property, and amenable band structure [5]. Although recent research has led to the identification of several transition metal-based electrocatalysts, a rational approach is still missing for

optimal catalyst surface design. An interesting approach to achieve this is by targeting transition metal-based coordination complexes (of Ni [6], Co [7], Cu [8], and Mn [9]) where the isolated metal–ligand core can provide significant insight into the intrinsic electrocatalytic activity of the transition metal site in presence of specific ligand environment, that can be then extrapolated into the extended solid.

In this regard, multimetallic molecular clusters can be highly interesting for such catalyst design. These molecular cluster comprising a large number of atoms in the building block serves as the link interconnecting solid state and molecular chemistry [10]. Among these, homometallic metal chalcogenide carbonyls [11,12], clusters containing metal rings and metal–metal bonds stabilized by either phosphines [13,14], or arenes [15], as well as the bridging chalcogenide [16] (μ_3-S [12,17], μ_3-Se [18], and μ_3-Te [13]) ligands are especially attractive due to the packing density and availability of multiple catalytic sites. Of particular interest is the selenium-capped carbonyltrimetallic cluster of which only very few have been reported [18–20]. The first three members of group 6B (Cr, Mo, and W) are known [18,19], and mixed metal [19,20] and Fe-based clusters have been reported [21]. Although some structural, magnetic, and optical studies have been reported [20–22], however, they have not been explored for electrochemical properties.

Despite the unique properties of chromium favoring catalytic properties, very few Cr-based compositions have been studied for electrocatalysis [23–26]. Chromium is a high valance transition-metal and being slightly oxophilic can easily associate with hydroxide ions of the electrolyte. The strength of the Cr-O bond is of significance in catalysis, since higher strength favors chemisorption and O-O bond activation [27]. Recently, a trichromium diselenium carbonyl complex, $[Se_2Cr_3(CO)_{10}](Et_4N)_2$, was reported [19], with a distinctive triangular metal bonding structure. This complex provides a unique opportunity for understanding the role and effect of the structure and bonding nature of the core Cr-Se bond, and the presence of Cr-Cr bonds on electrocatalytic water oxidation. The activity of the Cr-Se core in the cluster system could demonstrate the intrinsic activity of the Cr-Se linkages and by extension the activity of bulk Cr-based chalcogenides, and other coordination polymers with similar structures.

To date, the electrochemical OER activity of Cr-based molecular clusters has not been studied in any systematic investigations. Herein, we report the use of the Se-capped trichromium carbonyl cluster $[Se_2Cr_3(CO)_{10}](Et_4N)_2$ as a highly efficient electrocatalyst for water oxidation. The OER activity in an alkaline medium revealed a low onset potential of 1.47 V vs. RHE with an overpotential of 310 mV @ 10 mA cm^{-2}. This enhancement in electrocatalytic activity can be attributed to the optimal binding strength provided by catalytically active Cr sites, which is favorable for the adsorption of oxygen-containing intermediates, assisted by local oxidation of Cr(III) to (Cr(VI) during the polarization process.

2. Results

The Se-capped carbonyltrichromium $[Se_2Cr_3(CO)_{10}](Et_4N)_2$ molecular cluster was synthesized by reaction of $Cr(CO)_6$ with SeO_2 in concentrated methanolic-NaOH solution using cation metathesis with $[Et_4N]Br$, following reported procedure [19]. This reaction led to the formation of the Cr-Se complex as represented in Figure 1a which had a distinct red coloration and has been referred to as the red Cr-Se complex henceforth. The Cr-Se cluster has an interesting structure exhibiting trigonal bipyramidal coordination with bridging μ_3-Se atoms capped above and below bonded Cr_3-ring. In this bonding situation, each Se atom donates $4e^-$ to the Cr_3 triangle forming $48e^-$ species, which supports the Cr_3 having (3×) Cr-Cr bonds. The washings during the metathesis with $[Et_4N]Br$ were collected, concentrated, washed, and dried, yielding another Cr-Se complex with a distinct green coloration, referred to as a green Cr-Se cluster. The detailed crystal structure analysis of the Cr-Se red cluster from single crystal X-ray diffraction has been reported previously [19]. Raman and FTIR analysis were used to further characterize these Cr-Se complexes, specifically the green cluster.

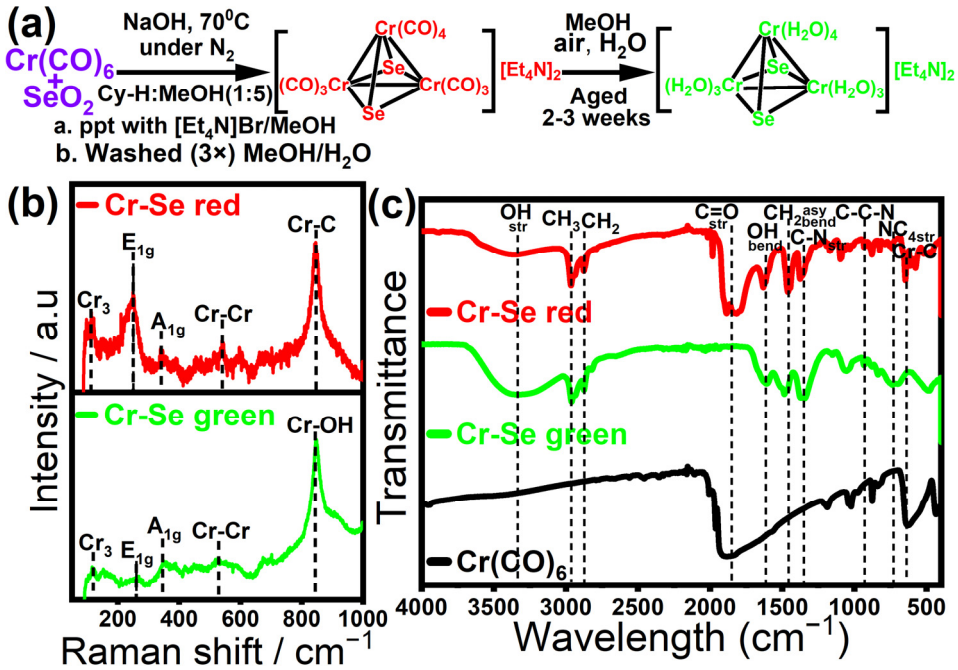

Figure 1. Synthesis and spectroscopic characterizations of Cr–Se red and Cr–Se green catalysts. (**a**) Reaction scheme describing synthesis method along with compositional details. (**b**) Raman spectra, excited with 632.8 nm HeNe laser radiation; (**c**) FTIR spectra.

The Raman spectra showed the presence of a Raman peak at 117 cm^{-1} corresponding to the Cr_3 motif, while peaks around 250 and 342 cm^{-1} were attributed to E_{1g} and A_{1g} modes in both clusters. The Raman peak at 847 cm^{-1} corresponds to the vibrational mode of Cr-C in the Cr-Se red cluster while the peak at 850 cm^{-1} indicated the presence of Cr-OH linkage in the Cr-Se green cluster Figure 1b. The FTIR spectra (Figure 1c) also showed broad IR peaks ~3461 cm^{-1} attributed to O-H stretching mode in both Cr-Se red and Cr-Se green clusters, indicating the presence of moisture. However, the peak was much broader and more intense in the Cr-Se green cluster, indicating the higher magnitude of hydrogen bonds, possibly due to the presence of coordinated H_2O molecules, while the IR peak ~1623 cm^{-1} could be assigned to the O-H bending mode of H_2O molecules. The Cr-Se green showed no peak between 1900–1550 cm^{-1} indicating the absence of the CO group, while Cr-Se red shows a doublet peak at around 1800 cm^{-1}, indicating the presence of a bound CO group [28]. Furthermore, the IR absorption vibrational peaks that appeared at 1461 cm^{-1} were assigned to CH_3 while 2963 cm^{-1} and 2877 cm^{-1} correlate with CH_3 and CH_2 modes, respectively, confirming the presence of Et_4N counter ions in these clusters [29–31]. The absorption peaks below 800 cm^{-1}, correspond to other bending and stretching vibration modes including Cr-Se at 668 cm^{-1}, while other less obvious peaks are most likely due to O-M-O and M-O-H modes. The CHN elemental analysis of the Cr-Se red and Cr-Se green cluster samples revealed the relative atomic ratio of C, H, and N in the samples (SI Experimental Section). Such compositional analysis also corroborated the formulation of the green cluster as $Cr_3Se_2C_{40}H_{117}N_5O_{10}$, while the red cluster had a molecular formula of $Cr_3Se_2C_{26}H_{40}N_2O_{10}$ as shown in Figure 1a. Specifically, the CO ligands coordinated to Cr in the red cluster were replaced with water molecules to form the green clusters.

X-ray photoelectron spectroscopy (XPS) was employed to characterize the oxidation states, composition, and local coordination of the cluster surface (Figure 2). Deconvoluted peaks of the Cr 2*p* spectrum (Figure 2a) showed peaks around 576.0 eV and 585.9 eV attributed to Cr(III) of $2p_{3/2}$ and $2p_{1/2}$ states, respectively, while two other peaks around 578.4 eV and 586.7 eV were matched to Cr(VI) of $2p_{3/2}$ and $2p_{1/2}$ states, respectively [1]. This indicates that Cr(III) and Cr(VI) states co-exist in the cluster, with Cr(III) as the main species. The Se 3d spectrum (Figure 2b) shows peaks at 53.3 and 54.6 eV assigned respectively to

Se $3d_{5/2}$ and Se $3d_{3/2}$, which corroborates the presence of Se^{2-}, whereas the low-intensity peak around ~58.6 eV corresponds to SeO_x species which could be from selenide surface oxidation [6,7,32]. Interestingly, XPS analysis revealed minimal Cr-oxide on the surface. The deconvoluted C 1*s* spectrum (Figure 2c) shows three peaks, corresponding to sp^3-C at around 284.8 eV, the C-O of carboxyl, or carbonyl groups at 286.1 eV, and the C=O of carbonyl groups at 288.8 eV. These were corroborated by the O1 s spectrum (Figure 2c) showing peaks corresponding to C=O and C-OH, in addition to Cr-C-O and Cr-O peaks.

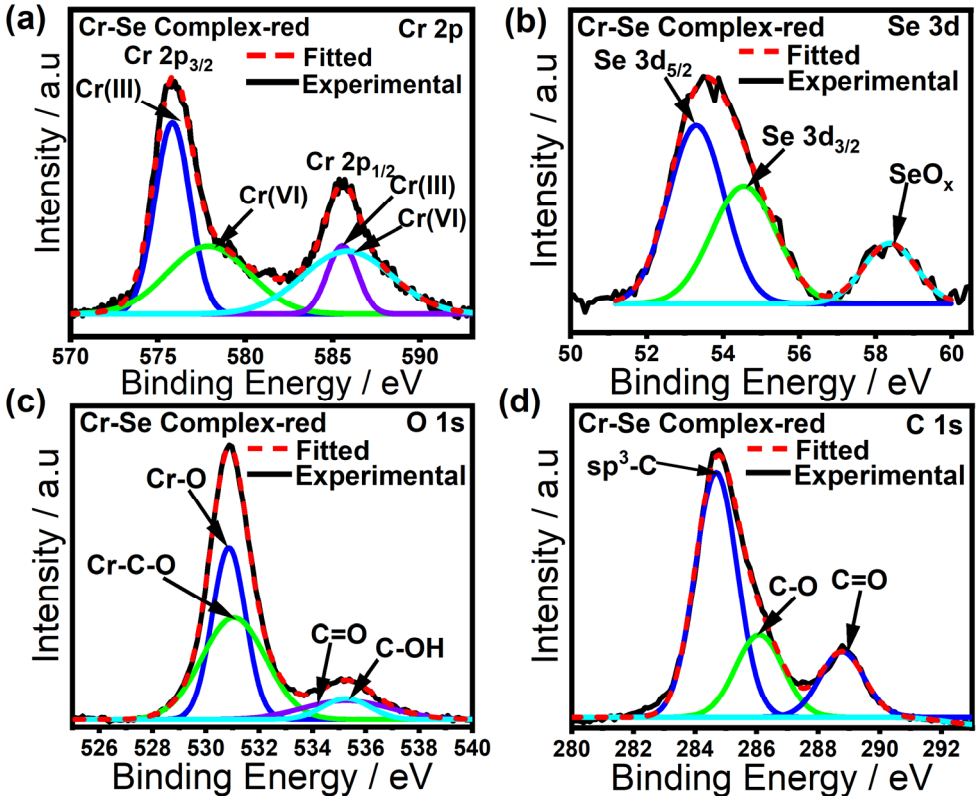

Figure 2. The high-resolution XPS spectra of Cr-Se red complex showing (**a**) Cr 2*p* peak; (**b**) Se 3d peak; (**c**) C s1 peak; (**d**) surface O 1s peak.

Similar observations were made for the Cr-Se green complex (Figure 3), where the high-resolution XPS spectra for Cr-Se green were measured to determine the valence states of the Cr species by the deconvolution of the Cr 2*p* spectrum. The peaks at 576.2 eV and 586.0 eV were assigned to Cr(III) $2p_{3/2}$ and Cr(VI) $2p_{1/2}$, respectively, while deconvoluted peaks at 574.1 eV and 574.4 eV were attributed to Cr(0) and Cr(II), respectively. The other two peaks at 576.3 eV and 583.0 eV were due to the presence of Cr(OH) and CrO_x, respectively. This is similar to what was observed in the previous report [33], indicating the formation of surface oxides and hydroxyl coordination in the cluster. However, Cr(III) was still observed as the dominant species. The Se 3d spectrum, showed peaks shifted to 57.6 and 58.6 eV corresponding to Se $3d_{5/2}$ and Se $3d_{3/2}$, respectively, which confirmed the presence of Se^{2-}. The peak at ~62.0 eV indicates the existence of SeO_x species which could arise from selenide surface oxidation. However, no metal oxides were detected on the catalyst surface from the XPS analysis. The C 1*s* spectra were deconvoluted and the peak at 284.9 eV corresponded to the sp^3-C bond, and the peak at 285.4 eV C-O bond of carboxyl or carbonyl functional groups, and the peak at 288.7 eV was assigned to C=O bond of carbonyl groups [1,23,24]. Furthermore, the thermogravimetric analysis (TGA) described the stepwise decomposition of both of Cr-Se red and Cr-Se green clusters (Figure S1), and the percentage weight loss in both complexes agree with the calculated values estimated from the proposed molecular formulation.

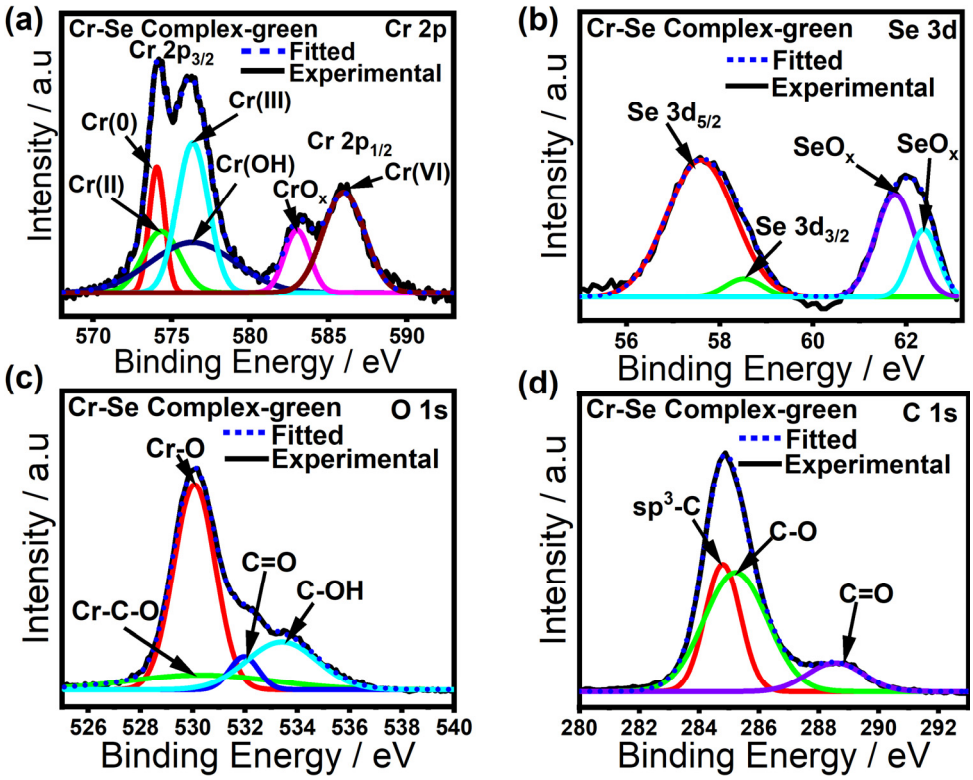

Figure 3. The high-resolution XPS spectra of Cr-Se green complex showing (**a**) Cr 2*p* peak; (**b**) Se 3d peak; (**c**) C s1 peak; (**d**) surface O 1s peak.

The electrocatalytic OER performance of Cr-Se red and Cr-Se green clusters was investigated in an alkaline medium of 1 M KOH (pH 13.7) using a three-electrode system, with graphite rod and Ag | AgCl as counter and reference electrodes, respectively, while the catalysts were drop casted on a conductive carbon paper and used as working electrode. The assembly of the catalyst electrode (working electrode preparation) is described in the materials and methods section. The polarization curves obtained using linear scan voltammetry (LSV) (Figure 4a) indicate that Cr-Se red cluster achieved an overpotential of 310 mV at 10 mA cm^{-2} making it a better OER active electrocatalyst in comparison to the Cr-Se green cluster with 350 mV overpotential. It can be observed that the presence of Cr in variable oxidation states in both samples strongly influences the OER performance by improving current density and minimizing overpotential. The presence of Cr in two different oxidation states, not only increases electroactive sites but further enhances the electronic transition, thereby facilitating catalyst activation through hydroxide adsorption on the Cr catalytic sites. Moreover, the higher covalency of the multiple Cr-Se bonds present as well as the enhanced conductivity of Cr-Cr bonds are important factors that could affect the observed catalytic efficiency. Additionally, the lability of the coordinating ligands in the Cr-Se green clusters tends to free up the metal sites for incoming OH^- under applied potential [34]. The activity of Cr-Se green was observed to be moderately good; this can be attributed to the association of Cr sites with water and OH- which has been demonstrated to show high intermediate adsorption on catalytic sites leading to performance enhancement [24]. The cyclic voltammetry (CV) shown in Figure 4b,c illustrates the reduction of the active Cr species during a reverse sweep at potentials of 1.33 and 1.35 vs. RHE for Cr-Se red and Cr-Se green clusters, respectively, which is consistent with reported literature [35]. The active species is regenerated in the forward oxidation sweep at potentials around 1.46 and 1.48 vs. RHE [36], just before the OER onset, further corroborating with the activity observed by the LSV (Figure 4a). The oxidation and reduction reaction kinetics of the Cr-Se red cluster was measured using variable scan rates between 10 and 100 mV/s in OER (Figure 4d). This shows more obvious reduction

peaks shifting slightly more left, while oxidation peaks shifting slightly more right indicate quasi-reversible behavior of Cr species [37].

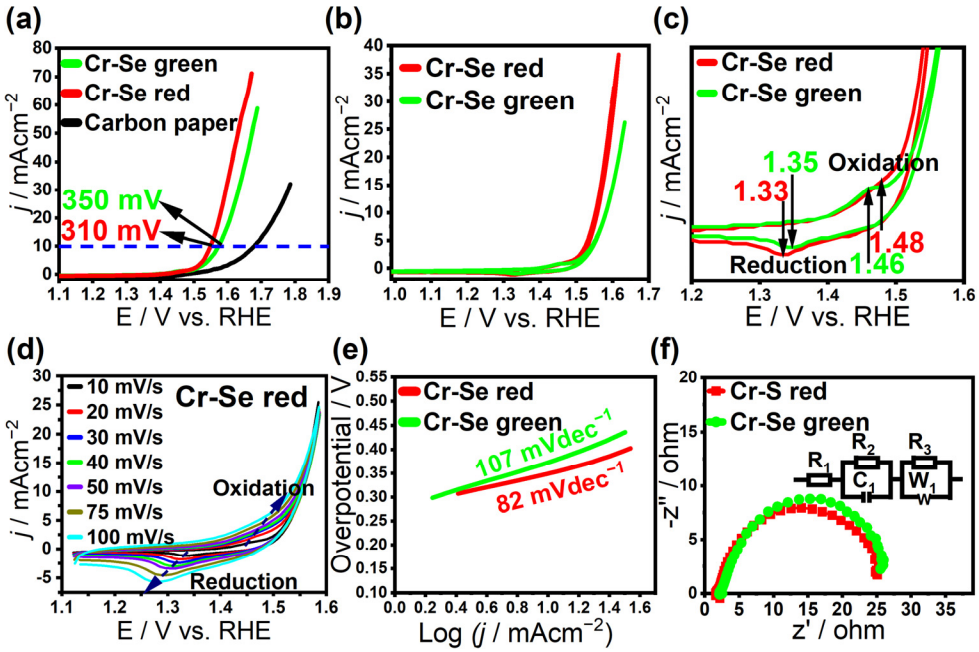

Figure 4. Electrocatalytic performance of Cr–Se red and Cr–Se green complexes. (**a**) Linear scan voltammetry showing overpotential at 10 mA/cm^2. (**b**) Cyclic voltammetry. (**c**) The Cr(III) and Cr(VI) redox potentials for Cr–Se red and green complexes. (**d**) Cyclic voltammograms of Cr–Se red complex measured at scan rates from 10 to 100 mV/s. (**e**) Tafel plots. (**f**) Electrochemical impedance spectroscopy (EIS) showing Nyquist plots in the AC frequency range between 100 kHz and 0.1 Hz, at 1.55 V vs. RHE. Inset shows the fitted equivalent circuit.

The Tafel slope for Cr-Se red was found to be 82 mV dec^{-1} as compared Cr-Se green, which was 107 mV dec^{-1}, which indicates a much faster reaction kinetics and simple electron transfer between the Cr-Se red electrocatalyst and electrolyte (Figure 4e), in agreement with the observation of facile OER. The electrochemical impedance spectroscopy (EIS) plots (Figure 4f) showed semi-circular ellipsoids, which could be fitted to equivalent circuit models depicting the various conducting pathways on the catalyst-electrode composite [38]. Typically, two processes can occur during electrochemical OER: (i) reactive intermediate adsorption through catalyst activation; and (ii) O-O desorption process. An equivalent circuit demonstrating two charge-transfer, a process obtained from EIS plot fitting, is shown in the insert in Figure 4f. The R_1 values are the electrolyte resistance. C_1R_2 represents the transformation of the active intermediate and W_2R_3 for the O-O desorption process. Table S1 shows EIS equivalent circuit parameters. The Cr-Se red revealed a smaller R_1 value indicating a faster charge-transfer process. The OER activity of both Cr-Se red and Cr-Se green molecular complexes were compared with the recently published Cr-based OER electrocatalysts as shown in Table S2 in supporting information. It was found that our catalysts were comparable to or better than the recently published Cr-based electrocatalysts which further confirms the critical influence of ligand coordination on electrocatalytic activity.

To further appreciate the OER activity of the Cr-Se red and Cr-Se green cluster electrocatalysts, the mass activity and turnover frequency (TOF) were obtained as shown in Figure 5. The OER-specific mass activities were measured at 0.39 V overpotential. Cr-Se red and Cr-Se green catalysts exhibit specific mass activities of 62.4 and 37.2 Ag^{-1}, respectively (Figure 5a). Furthermore, the TOF of 0.0174 and 0.0164 s^{-1} was achieved at 0.39 overpotential for Cr-Se red and Cr-Se green catalysts, respectively.

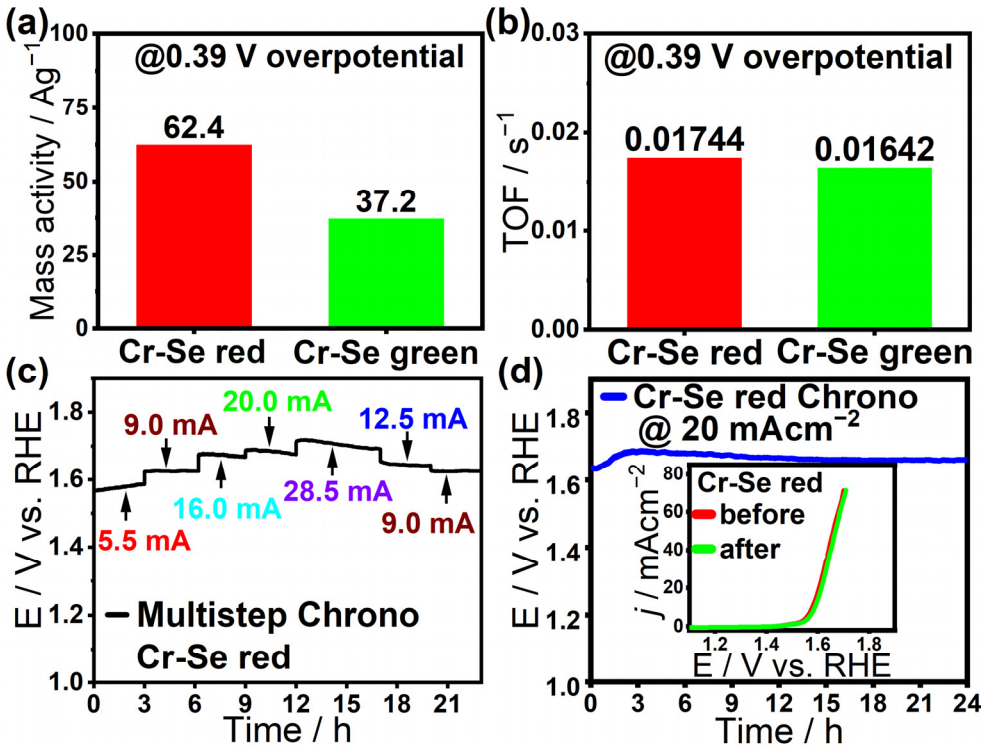

Figure 5. Electrocatalytic performance of Cr–Se red and Cr–Se green complexes. (**a**) Mass activity; (**b**) Turnover frequency (TOF); (**c**) Multistep chronoamperometry study of Cr–Se red at various current densities.; (**d**) Chronoamperometry at constant current density. Inset shows the comparison of OER activity before and after long-term chronoamperometry.

The electrochemically active surface area (ECSA) is one of the key descriptors for electrocatalysts which influences the kinetics of electrochemical conversion. The ECSAs of Cr-Se red and Cr-Se green were investigated using cyclic voltammetry (CV) plots collected in the range from 0.05 to 0.25 V vs. Ag | AgCl with scan rates between 20 and 100 mV s^{-1} in N_2 saturated 1 M KOH solution. Figures S2 and S3 show the anodic and cathodic currents plotted as a function of scan rates. ECSA was calculated using the double-layer capacitance of the catalysts and the specific capacitance as described in the Experimental Section. Cr-Se red and Cr-Se green clusters showed ECSA of 91 cm^2 and 54 cm^2, respectively, corroborating the accessibility to a larger number of active sites and hence the high activity observed.

The electrochemical OER parameters of Cr-Se red and Cr-Se green are compared in Table 1. The Cr-Se red shows lower overpotential and Tafel slope, indicating better electrocatalytic activity. In addition, its TOF, mass activity, and ECSA were higher for the Cr-Se red, further corroborating its higher performance. A higher ECSA value generally indicates a larger electrochemically active surface area which improves electrolyte/active site interaction, leading to better catalytic performance for OER. A large ECSA value results in high surface roughness (RF), which is another parameter considered that affects catalytic activity. The steady-state performance and long-term durability were tested by chronopotentiometry for the most active Cr-Se complex OER electrocatalyst. The multistep chronoamperometry stability test for Cr-Se red cluster at different current densities between 5 mA cm^{-2} and 30 mA cm^{-2} showed no obvious degradation in potential under the tested current density (Figure 5c), suggesting that the Cr-Se red cluster is highly stable under a wide range of current densities, exhibiting robustness toward longevity in OER.

Table 1. Electrocatalytic parameters compared in Cr-Se catalytic systems.

Material	Cr-Se Red	Cr-Se Green
Onset potential (V) vs. RHE	1.47	1.58
Overpotential @ 10 mA cm^{-2} (mV)	310	350
TOF (s^{-1}) @ 0.39 V	0.0174	0.0164
Mass activity (Ag^{-1}) @ 0.39 V	62.4	37.2
Tafel slope (mV dec^{-1})	82	107
ECSA (cm^{-2})	289	139
RF	1023	492

Furthermore, chronoamperometry sustained at 20 mA cm^{-2} current density for a 24 h period and shows no significant change in the activity as shown in Figure 5d. This confirms that the Cr-Se red cluster material is highly active towards OER as well as durable over a long activity period under an alkaline medium. In the Cr-Se red catalyst, a decrease in the Cr-CO (847 cm^{-1}) peak signal and an increase in the Cr-OH (850 cm^{-1}) peak signal was observed, and a formation of a shoulder at ~900 cm^{-1} corresponding to O-Cr-O after chronoamperometry (Figure 6). This could be from the adsorption of the OH ion on the surface of the catalyst. The Cr-Se green after chronoamperometry shows a more pronounced A_{1g} (378 cm^{-1}) due to the formation of surface chromium-hydroxide linkage, Cr-OH peak signal (850 cm^{-1}), illustrating more OH adsorption on the catalytic site [39–41]. However, the catalyst characterization after chronoamperometry shows minimal surface oxidation as demonstrated by the XPS in Figures S4 and S5, further corroborating the stability of these complexes while catalytic sites underwent local activation through intermediate adsorption. Moreover, no significant surface-leaching structural changes were observed after the stability study.

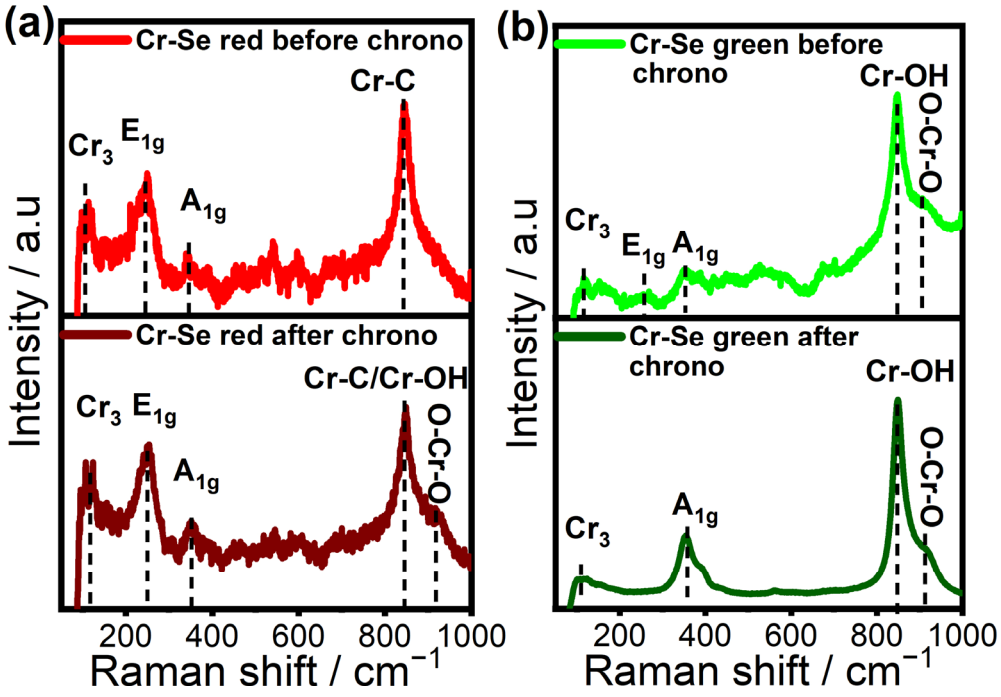

Figure 6. Raman spectra, excited with 632.8 nm HeNe laser radiation of (**a**) Cr–Se red complex before and after chronoamperometry study; (**b**) Cr–Se green complex before and after chronoamperometry study.

3. Materials and Methods

Conductive carbon paper (CCP) suitable for battery, fuel cell, and supercapacitor research were purchased from MSE supplies, Tucson, AZ 85711 USA. Chromium hexacarbonyl, Nafion (5 wt.%), selenium (IV) oxide (SeO_2), isopropanol (iPr-OH), and cyclohexane

(C_6H_{12}) were purchased from Sigma–Aldrich Chemical Reagent Co., Ltd. St. Louis MO, sodium hydroxide (NaOH), methanol (MeOH), dichloromethane (CH_2Cl_2), and tetraethyl bromide [Et_4N]Br were purchased from Fisher Scientific Pittsburgh, USA. All the reagents were used as received. The deionized (DI) water purified through a Millipore system was used in all experiments. The CCP was washed with iPr-OH and DI water several times to ensure the surface is cleaned before use.

3.1. Preparation of Cr-Se Red Complex

The synthesis of Cr-Se red (decacarbonyltrichromium diselenide ditetraethylamine) compound has been reported in a previous report [19]. All reactions were carried out under the N_2 atmosphere. A mixed solution of MeOH (30 mL) and cyclohexane (7.5 mL) was added to a mixture containing [$Cr(CO)_6$] (0.8 g, 3.64 mmol), SeO_2 (0.21 g, 1.89 mmol), and NaOH (3.0 g, 82.5 mmol) taken in 100 mL three neck round flask. This mixture was heated to reflux at 70 °C for 12 h, yielding a dark-red solution that was filtered, and the filtrate was concentrated. A MeOH solution of [Et_4N]Br (3.0 g, 14.3 mmol) was added to the concentrated filtrate dropwise, whereby the red $Cr_3Se_2(CO)_{10}](Et_4N)_2$ was precipitated as a solid product in a metathesis reaction. The solid product was washed several times with MeOH and CH_2Cl_2 and dried as Cr-Se red complex. Elemental analysis found the following composition for Cr-Se red: C, 36.20; H, 5.61; N, 3.28%. Calculated: C, 36.55; H, 4.72; N, 3.28%. Compound Cr-Se red is soluble in MeCN and acetone, but insoluble in other organic solvents.

3.2. Preparation of Cr-Se Green Complex

The Cr-Se green (decahydrate trichromium diselenide ditetraethylamine) was accidentally formed from Cr-Se red, by leaving the Cr-Se red solid product to remain standing in MeOH and CH_2Cl_2 during washing for 2–3 weeks in the presence of moisture and air, and was dried as Cr-Se green complex. Elemental analysis found for Cr-Se green: C, 28.28; H, 7.91; N, 1.83%. Calculated: C, 25.47; H, 8.01; N, 3.71%. Compound Cr-Se green is soluble in MeCN and acetone, but insoluble in other organic solvents.

3.3. Electrode Preparation

All CCP substrates were cleaned with iPr-OH, dried, and covered with Teflon tape, leaving an exposed geometric area of 0.283 cm^2. Catalyst ink was prepared by dispersing 10.0 mg of the catalyst in 1.0 mL 0.8% Nafion in iPr-OH and ultrasonicated for 30 min. A 20 µL volume of the ink was pipetted out and drop casted on the CCP substrate on the exposed geometric area, dried at room temperature, and finally heated at 130 °C in an oven for 30 min in air. This was used as working electrodes.

3.4. Characterization Methods

XPS measurements were performed using a KRATOS AXIS 165 X-ray photoelectron spectrometer (Kratos Analytical Limited, Manchester, UK) using a monochromatic Al X-ray source. The C 1s signal at 284.5 eV was used as a reference to correct all the XPS binding energies [7]. All XPS spectra were collected from the pristine catalyst surface without sputtering. The Raman spectra of the catalyst were recorded with LabRam ARAMIS (HORIBA Jobin-Yvon Raman spectrometer equipped with a CCD detector) in the Raman shift range between 50 cm^{-1} and 1800 cm^{-1}, 1200 lines mm^{-1} grating, HeNe laser 632.8 nm excitation with a nominal output power of 100 mW, 0.95 cm^{-1}/pixel spectral dispersion, 10% of laser power, 10× objective, 0.25 numerical aperture, 100 µm slit, 200 µm hole, 30 s exposure time, and 10× accumulations for each sample acquisition [42]. Fourier Transform Infrared (FTIR) spectra were recorded using a Thermo Nicolet NEXUS 470 FT-IR Spectrometer, in a range of 400–4000 cm^{-1} with 1 cm^{-1} resolution. Pellets were prepared by pressing a mixture of 2 mg catalyst and 200 mg KBr under a load of 10–15 tons [43,44]. Thermal gravimetric analysis (TGA) was performed with a heating rate of 10 °C min^{-1} on a Netzsch STA 449C instrument [33].

Electrochemical measurements were performed using a conventional three-electrode system connected to an IviumStat potentiostat, with catalyst-coated CCP as the working electrode, while graphite rod and Ag/AgCl electrode were used as counter electrode and reference electrodes, respectively, to measure the electrocatalytic performances. Linear sweep voltammetry (LSV) and cyclic voltammetry (CV) were carried out to study the OER catalytic performance and cycling stability. To reduce uncompensated solution resistance, all activity data were iR-corrected, which was measured through electrochemical impedance studies.

All potentials measured were calibrated to RHE using the following Equation (1):

$$E_{(RHE)} = E_{(Ag/AgCl)} + 0.197V + 0.059*pH \quad (1)$$

All electrolytes were saturated by oxygen (for OER) bubbles before and during the experiments.

3.5. Chronoamperometry Stability Study

The steady-state performance and durability of Cr-Se red electrocatalysts in OER for long-term chronoamperometric stability in the alkaline electrolyte of 1 M KOH solution were carried out in two forms: (a) At a constant current density of 20 mA·cm^{-2} for 24 h. (b) At various current densities between 5 and 30 mA·cm^{-2} as multistep study, both in N_2-saturated 1.0 M KOH at room temperature.

3.6. Tafel Slope

The Tafel slope, an important parameter to explain the electrokinetic activity of these thin film catalysts for OER and HER processes, was estimated from the Tafel plot. The Tafel equation is given as the dependence of overpotential η on the current density *j* as shown in Equation (2)

$$\eta = \alpha + (2.3RT/\alpha nF) * \log (j) \quad (2)$$

where α is the transfer coefficient, *n* is the number of electrons involved in the reaction, and *F* is the Faraday constant. The Tafel slope is given by (2.3RT/αnF). The Tafel plots in this work were calculated from the reverse scan of CV collected at a scan rate of 2 mV s^{-1} in a non-stirred N_2-saturated 1.0 M KOH solution.

3.7. Electrochemical Impedance Spectroscopy (EIS)

The EIS experiments were performed within 10^5–10^{-2} Hz frequency range, at an AC signal amplitude of 10 mV, to study the electrode kinetics and estimate the electrolyte resistance (R_1), charge transfer resistance at the electrode (catalyst)-electrolyte interface (R_2), as well as the film resistance (R_3). The Nyquist plots were collected in N_2-saturated 1.0 M KOH at an applied potential of 0.55 V vs. Ag | AgCl (KCl saturated).

3.8. Turnover Frequency (TOF)

Turnover frequency (TOF) for the electrocatalysts was calculated from Equation (3):

$$TOF = j*A/4*m*F \quad (3)$$

where *j* is the current density in mA cm^{-2} at a given overpotential (e.g., η = 0.39 V), A is the surface area of the electrode (0.283 cm^2), F is the Faraday constant (a value of 96,485 C mol^{-1}), and m is moles of catalyst on the electrode.

3.9. Mass Activity

Mass activity (A g^{-1}) is the current density per unit mass of the active catalyst at a given overpotential. This is calculated from catalyst loading m and the measured current density j (mA cm^{-2}) of the catalyst, at η = 0.39 V, calculated from Equation (4).

$$\text{Mass activity} = j/m \quad (4)$$

3.10. Electrochemically Active Surface Area (ECSA) and Roughness Factor (RF)

The electrochemically active surface area (ECSA) of the catalyst was estimated by measuring the electrochemical double-layer capacitance (C_{DL}) at different scan rates in the non-Faradaic region. It was assumed that the current obtained in the non-Faradaic region is caused by double-layer charging instead of electrochemical reactions or charge transfer. The double-layer current (i_{DL}) was obtained by performing cyclic voltammograms (CVs) with various scan rates in a non-stirred N_2 saturated 1.0 M KOH solution. The ratio of double-layer current (i_{DL}) and the scan rate (ν) of CV yielded the specific electrochemical double-layer capacitance (C_{DL}). Averaging of cathodic and anodic slopes gave absolute values obtained from the CV plot in the non-faradaic region as described in Equation (5).

$$i_{DL} = C_{DL} * V \quad (5)$$

The ECSA of the catalyst was calculated using Equation (6) where C_S is the specific capacitance as reported in alkaline solution to be between 0.022 and 0.130 mF cm^{-2} in alkaline solution. In this study, we assumed the value of C_S to be = 30 μFcm^{-2} based on previously reported OER catalysts in an alkaline medium.

$$ECSA = C_{DL}/C_S \quad (6)$$

The roughness factor (RF) is another important parameter that defines catalyst surface roughness and can influence observed catalytic properties. It is estimated as the ratio of ECSA and the geometric electrode area (0.283 cm^2) as shown in Equation (7).

$$RF = ECSA/SA \quad (7)$$

4. Conclusions

In essence, we have successfully demonstrated the use of a selenium-capped trichromium carbonyl $[Se_2Cr_3(CO)_{10}](Et_4N)_2$ cluster for the first time as an efficient, high performance, and stable electrocatalyst for OER. This Cr-Se red cluster consists of a catalytically active Se-Cr-Se coordinated sphere which shows high intrinsic catalytic activity supported by its low overpotential and Tafel slope of 310 mV at 10 mA cm^{-2} and 82 mV dec^{-1}, respectively, as well as high TOF (0.0174 s^{-1}) and mass activity (62.4 Ag^{-1}). It also showed excellent stability over 24 h in alkaline (1 M KOH) electrolytes. This indicates the promising potential of high-valence metal complexes and by extension their bulk solids with similar structural composition as highly active electrocatalysts in OER. The covalency of the multiple Cr-Se bonds in the cluster as well as the enhanced conductivity of Cr-Cr bonds are associated with the observed high catalytic efficiency. We believe that the presence of Cr in two different oxidation states, not only increases electroactive sites but further enhances the electronic transition. This facilitates the intermediate hydroxide adsorption on the Cr atoms, thus improving the electrocatalytic activity. These current findings provide a new avenue to explore the electrocatalytic applications of clustered high-valence metal complexes, as there is no systematic study reported for these cluster types in OER and other electrochemical energy conversions.

Supplementary Materials: The following supporting information can be downloaded at: https://www.mdpi.com/article/10.3390/catal13040721/s1, Figure S1: The thermogravimetric (TGA) analysis of (a) Cr-Se red; (b) Cr-Se green; Figure S2: Cr-Se red catalyst; (a) Cyclic voltammograms measured at different scan rates; (b) The plots of anodic and cathodic currents measured as a function of scan rate.; Figure S3: Cr-Se green catalyst; (a) Cyclic voltammograms measured at different scan rates; (b) The plots of anodic and cathodic currents measured as a function of scan rate; Figure S4: The high-resolution XPS spectra of the Cr-Se red complex after stability showing (a) Cr 2*p* peak; (b) Se 3d peak; (c) surface O 1s peak; (d) C s1 peak. Figure S5: The high-resolution XPS spectra of the Cr-Se green complex after stability showing (a) Cr 2*p* peak; (b) Se 3d peak; (c) surface O 1s peak; (d) C s1 peak. Table S1: Parameters of equivalent circuit obtained from fitting of EIS experimental data.

Table S2: Comparison of the OER performances in an alkaline electrolyte (overpotential at 10 mA cm^{-2} current density, and Tafel slope) of recently published chromium-based catalysts with our work. Refs. [16,25,45–52] are cited in the supplementary materials.

Author Contributions: Conceptualization, I.M.A. and M.N.; methodology, I.M.A. and M.N.; formal analysis I.M.A.; writing—original draft preparation, I.M.A.; writing—review and editing, I.M.A. and M.N.; supervision, M.N.; funding acquisition, M.N. All authors have read and agreed to the published version of the manuscript.

Funding: This research was funded by National Science Foundation, grant number CAS-2102609 and CAS 2155175.

Data Availability Statement: The research data will be made available directly from the authors upon request.

Acknowledgments: The authors would like to acknowledge Richard Brow at Materials Research Center, Missouri S & T for help with Raman spectroscopy.

Conflicts of Interest: The authors declare no conflict of interest.

References

1. Khatun, S.; Roy, P. Cobalt Chromium Vanadium Layered Triple Hydroxides as an Efficient Oxygen Electrocatalyst for Alkaline Seawater Splitting. *Chem. Commun.* **2022**, *58*, 1104–1107. [CrossRef] [PubMed]
2. Roy, S.B.; Akbar, K.; Jeon, J.H.; Jerng, S.K.; Truong, L.; Kim, K.; Yi, Y.; Chun, S.H. Iridium on Vertical Graphene as an All-Round Catalyst for Robust Water Splitting Reactions. *J. Mater. Chem. A Mater.* **2019**, *7*, 20590–20596. [CrossRef]
3. Lee, Y.; Suntivich, J.; May, K.J.; Perry, E.E.; Shao-Horn, Y. Synthesis and Activities of Rutile IrO_2 and RuO_2 Nanoparticles for Oxygen Evolution in Acid and Alkaline Solutions. *J. Phys. Chem. Lett.* **2012**, *3*, 399–404. [CrossRef] [PubMed]
4. Antolini, E. Iridium as Catalyst and Cocatalyst for Oxygen Evolution/Reduction in Acidic Polymer Electrolyte Membrane Electrolyzers and Fuel Cells. *ACS Catal.* **2014**, *4*, 1426–1440. [CrossRef]
5. Hong, W.T.; Risch, M.; Stoerzinger, K.A.; Grimaud, A.; Suntivich, J.; Shao-Horn, Y. Toward the Rational Design of Non-Precious Transition Metal Oxides for Oxygen Electrocatalysis. *Energy Environ. Sci.* **2015**, *8*, 1404–1427. [CrossRef]
6. Masud, J.; Ioannou, P.C.; Levesanos, N.; Kyritsis, P.; Nath, M. A Molecular Ni-Complex Containing Tetrahedral Nickel Selenide Core as Highly Efficient Electrocatalyst for Water Oxidation. *ChemSusChem* **2016**, *9*, 3128–3132. [CrossRef] [PubMed]
7. Abdullahi, I.M.; Masud, J.; Ioannou, P.-C.; Ferentinos, E.; Kyritsis, P.; Nath, M. A Molecular Tetrahedral Cobalt–Seleno-Based Complex as an Efficient Electrocatalyst for Water Splitting. *Molecules* **2021**, *26*, 945. [CrossRef]
8. Geer, A.M.; Musgrave, C.; Webber, C.; Nielsen, R.J.; McKeown, B.A.; Liu, C.; Schleker, P.P.M.; Jakes, P.; Jia, X.; Dickie, D.A.; et al. Electrocatalytic Water Oxidation by a Trinuclear Copper(II) Complex. *ACS Catal.* **2021**, *11*, 7223–7240. [CrossRef]
9. Najafpour, M.M.; Allakhverdiev, S.I. Manganese Compounds as Water Oxidizing Catalysts for Hydrogen Production via Water Splitting: From Manganese Complexes to Nano-Sized Manganese Oxides. *Int. J. Hydrogen Energy* **2012**, *37*, 8753–8764. [CrossRef]
10. Schmid, G. *Clusters and Colloids. From Theory to Applications*; VCH Verlagsgesellschaft: Weinheim, Germany, 1994; ISBN 0195069005.
11. Darensbourg, D.J.; Zalewski, D.J.; Sanchez, K.M.; Delord, T. Cluster Synthesis via Aggregation: Synthesis and Solution and Solid-State Characterization of Sulfur-Capped Group 6 Metal Carbonyl Clusters. *Inorg. Chem.* **1988**, *27*, 821–829. [CrossRef]
12. Hoefler, M.; Tebbe, K.-F.; Veit, H.; Weiler, N.E. Synthesis and Structure of [PPN]2[M2-CO)3(CO)9Cr3(M4-S)Cr(CO)5]: A Chromium Cluster. *J. Am. Chem. Soc.* **1983**, *3*, 6338–6339. [CrossRef]
13. Hessen, B.; Siegrist, T.; Palstra, T.; Tanzler, S.M.; Steigerwald, M.L. $Cr_6Te_8(PEt_3)_6$ and a Molecule-Based Synthesis of Cr_3Te_4. *Inorg. Chem.* **1993**, *32*, 5165. [CrossRef]
14. Tsuge, K.; Imoto, H.; Saito, T. Syntheses, Structures, and Molecular-Orbital Calculations of Chromium Chevrel-Type Cluster Complexes $[Cr_6E_8(PR_3)_6]$ (E=S, PR_3=PEt_3, PMe_3; E=Se, PR_3=PEt_3, PMe_3, PMe_2Ph). *Bull. Chem. Soc. Jpn.* **1996**, *69*, 627–636. [CrossRef]
15. Wang, W.; Wang, X.; Zhang, Z.; Yuan, N.; Wang, X. The Long-Sought Seventeen-Electron Radical $[(C_6Me_6)Cr(CO)_3]^+$: Isolation, Crystal Structure and Substitution Reaction. *Chem. Commun.* **2015**, *51*, 8410–8413. [CrossRef]
16. Bügel, P.; Krummenacher, I.; Weigend, F.; Eichhöfer, A. Experimental and Theoretical Evidence for Low-Lying Excited States in $[Cr_6E_8(PEt_3)_6]$ (E = S, Se, Te) Cluster Molecules. *Dalton Trans.* **2022**, *51*, 14568–14580. [CrossRef]
17. Darensbourg, D.J.; Zalewskl, D.J. Synthesis and Characterization of Sulfur-Capped Trlnuclear Group 6B Metal Clusters. *Organometallics* **1984**, *3*, 1598–1600. [CrossRef]
18. Hsu, M.H.; Miu, C.Y.; Lin, Y.C.; Shieh, M. Selenium-Capped Trimolybdenum and Tritungsten Carbonyl Clusters $[Se_2M_3(CO)_{10}]^{2-}$ (M = Mo, W). *J. Organomet. Chem.* **2006**, *691*, 966–974. [CrossRef]
19. Shieh, M.; Ho, L.F.; Jang, L.F.; Ueng, C.H.; Peng, S.M.; Liu, Y.H. First Selenium-Capped Carbonyltrichromium Complex $[Se_2Cr_3(CO)_{10}]^{2-}$: A Novel Cr_3 Ring Cluster. *Chem. Commun.* **2001**, *3*, 1014–1015. [CrossRef]
20. Shieh, M.; Lin, C.N.; Miu, C.Y.; Hsu, M.H.; Pan, Y.W.; Ho, L.F. Chromium-Manganese Selenide Carbonyl Complexes: Paramagnetic Clusters and Relevance to C = O Activation of Acetone. *Inorg. Chem.* **2010**, *49*, 8056–8066. [CrossRef]

21. Shieh, M.; Chung, R.L.; Yu, C.H.; Hsu, M.H.; Ho, C.H.; Peng, S.M.; Liu, Y.H. The Unusual Paramagnetic Mixed-Metal Carbonyl Chalcogenide Clusters: $[E_2Cr_2Fe(CO)_{10}]^{2-}$ (E = Te, Se). *Inorg. Chem.* **2003**, *42*, 5477–5479. [CrossRef]
22. Yeh, H.H.; Hsu, M.C.; Li, Y.H.; Hsu, Y.N.; Shr, F.Y.; Shieh, M. Ternary Antimony–Chalcogen Iron Carbonyl Complexes and Their Derivatives: Syntheses, Structures, Reactivities, and Low-Energy-Gap Characteristics. *J. Organomet. Chem.* **2021**, *937*, 121717. [CrossRef]
23. Jin, D.; Kang, J.; Prabhakaran, S.; Lee, Y.; Kim, M.H.; Kim, D.H.; Lee, C. Chromium-Rich $Cr_xIr_{1-x}O_2$ Wire-in-Tube Alloys for Boosted Water Oxidation with Long Standing Electrocatalytic Activity. *J. Mater. Chem. A Mater.* **2022**, *10*, 13803–13813. [CrossRef]
24. Kong, S.; Lu, M.; Yan, S.; Zou, Z. High-Valence Chromium Accelerated Interface Electron Transfer for Water Oxidation. *Dalton Trans.* **2022**, *51*, 16890–16897. [CrossRef] [PubMed]
25. Lin, C.C.; McCrory, C.C.L. Effect of Chromium Doping on Electrochemical Water Oxidation Activity by $Co_{3-x}Cr_xO_4$ Spinel Catalysts. *ACS Catal.* **2017**, *7*, 443–451. [CrossRef]
26. Du, X.; Su, H.; Zhang, X. Cr Doped-Co9S8 Nanoarrays as High-Efficiency Electrocatalysts for Water Splitting. *J. Alloys Compd.* **2020**, *824*, 153965. [CrossRef]
27. Moltved, K.A.; Kepp, K.P. The Chemical Bond between Transition Metals and Oxygen: Electronegativity, d-Orbital Effects, and Oxophilicity as Descriptors of Metal-Oxygen Interactions. *J. Phys. Chem. C* **2019**, *123*, 18432–18444. [CrossRef]
28. Shufler, L.; Sternberg, H.W.; Friedel, R.A. Infrared Spectrum and Structure of Chromium Hexacarbonyl, $Cr(CO)_6$. *J. Am. Chem. Soc.* **1956**, *78*, 2687–2688. [CrossRef]
29. Thalassinos, G.; Stacey, A.; Dontschuk, N.; Murdoch, B.J.; Mayes, E.; Girard, H.A.; Abdullahi, I.M.; Thomsen, L.; Tadich, A.; Arnault, J.-C.; et al. Fluorescence and Physico-Chemical Properties of Hydrogenated Detonation Nanodiamonds. *C J. Carbon Res.* **2020**, *6*, 7. [CrossRef]
30. He, T.; Zhou, T.; Wan, Y.; Tan, T. A Simple Strategy Based on Deep Eutectic Solvent for Determination of Aflatoxins in Rice Samples. *Food Anal. Methods* **2020**, *13*, 542–550. [CrossRef]
31. Amirthaganesan, G.; Kandhaswamy, M.A.; Srinivasan, V. Thermal, Phase Transition and FTIR Spectroscopic Studies in Tetraethylammonium Trichlorocadmiate Crystals. *Cryst. Res. Technol.* **2005**, *40*, 680–683. [CrossRef]
32. Swesi, A.T.; Masud, J.; Nath, M. Nickel Selenide as a High-Efficiency Catalyst for Oxygen Evolution Reaction. *Energy Environ. Sci.* **2016**, *9*, 1771–1782. [CrossRef]
33. Liu, B.; Han, W.; Li, X.; Li, L.; Tang, H.; Lu, C.; Li, Y.; Li, X. Quasi Metal Organic Framework with Highly Concentrated Cr_2O_3 Molecular Clusters as the Efficient Catalyst for Dehydrofluorination of 1,1,1,3,3-Pentafluoropropane. *Appl. Catal. B* **2019**, *257*, 117939. [CrossRef]
34. Ghosh, T.; Maayan, G. Efficient Homogeneous Electrocatalytic Water Oxidation by a Manganese Cluster with an Overpotential of Only 74 MV. *Angew. Chem. Int. Ed.* **2019**, *58*, 2785–2790. [CrossRef]
35. Stern, C.M.; Jegede, T.O.; Hulse, V.A.; Elgrishi, N. Electrochemical Reduction of Cr(vi) in Water: Lessons Learned from Fundamental Studies and Applications. *Chem. Soc. Rev.* **2021**, *50*, 1642–1667. [CrossRef] [PubMed]
36. Bose, R.N.; Fonkeng, B.; Barr-David, G.; Farrell, R.P.; Judd, R.J.; Lay, P.A.; Sangster, D.F. Redox Potentials of Chromium(V)/(IV),-(V)/(III), and -(IV)/(III) Complexes with 2-Ethyl-2-Hydroxybutanoato(2-/1-) Ligands. *J. Am. Chem. Soc.* **1996**, *118*, 7139–7144. [CrossRef]
37. Guziejewski, D.; Stojanov, L.; Gulaboski, R.; Mirceski, V. Reversible and Quasireversible Electron Transfer under Conditions of Differential Square-Wave Voltammetry. *J. Phys. Chem. C* **2022**, *126*, 5584–5591. [CrossRef]
38. Bo, X.; Li, Y.; Chen, X.; Zhao, C. High Valence Chromium Regulated Cobalt-Iron-Hydroxide for Enhanced Water Oxidation. *J. Power Sources* **2018**, *402*, 381–387. [CrossRef]
39. Zhang, B.; Zhang, B.; Zhao, G.; Wang, J.; Liu, D.; Chen, Y.; Xia, L.; Gao, M.; Liu, Y.; Sun, W.; et al. Atomically Dispersed Chromium Coordinated with Hydroxyl Clusters Enabling Efficient Hydrogen Oxidation on Ruthenium. *Nat. Commun.* **2022**, *13*, 5894. [CrossRef]
40. Gomes, A.S.O.; Yaghini, N.; Martinelli, A.; Ahlberg, E. A Micro-Raman Spectroscopic Study of $Cr(OH)_3$ and Cr_2O_3 Nanoparticles Obtained by the Hydrothermal Method. *J. Raman Spectrosc.* **2017**, *48*, 1256–1263. [CrossRef]
41. Huang, Y.M.; Tsai, H.R.; Lai, S.H.; Lee, S.J.; Chen, I.C.; Huang, C.L.; Peng, S.M.; Wang, W.Z. Bonding between Chromium Atoms in Metal-String Complexes from Raman Spectra and Surface-Enhanced Raman Scattering: Vibrational Frequency of the Chromium Quadruple Bond. *J. Phys. Chem. C* **2011**, *115*, 13919–13926. [CrossRef]
42. Abdullahi, I.M.; Langenderfer, M.; Shenderova, O.; Nunn, N.; Torelli, M.D.; Johnson, C.E.; Mochalin, V.N. Explosive Fragmentation of Luminescent Diamond Particles. *Carbon N. Y.* **2020**, *164*, 442–450. [CrossRef] [PubMed]
43. Saleh, T.A.; Al-Hammadi, S.A.; Abdullahi, I.M.; Mustaqeem, M. Synthesis of Molybdenum Cobalt Nanocatalysts Supported on Carbon for Hydrodesulfurization of Liquid Fuels. *J. Mol. Liq.* **2018**, *272*, 715–721. [CrossRef]
44. Beltz, J.; Pfaff, A.; Abdullahi, I.M.; Cristea, A.; Mochalin, V.N.; Ercal, N. Effect of Nanodiamond Surface Chemistry on Adsorption and Release of Tiopronin. *Diam. Relat. Mater.* **2019**, *100*, 107590. [CrossRef] [PubMed]
45. Gao, H.; Li, J.; Lian, K. Alkaline Quaternary Ammonium Hydroxides and Their Polymer Electrolytes for Electrochemical Capacitors. *RSC Adv.* **2014**, *4*, 21332–21339. [CrossRef]
46. Bo, X.; Li, Y.; Chen, X.; Zhao, C. Operando Raman Spectroscopy Reveals Cr-Induced-Phase Reconstruction of NiFe and CoFe Oxyhydroxides for Enhanced Electrocatalytic Water Oxidation. *Chem. Mater.* **2020**, *32*, 4303–4311. [CrossRef]

47. Ramakrishnan, P.; Beom Lee, K.; Choi, G.J.; Park, I.K.; Inn Sohn, J. Porous Hollow Nanorod Structured Chromium-Substituted Inverse Spinel Compound: An Efficient Oxygen Evolution Reaction Catalyst. *J. Ind. Eng. Chem.* **2021**, *101*, 178–185. [CrossRef]
48. Shifa, T.A.; Mazzaro, R.; Morandi, V.; Vomiero, A. Controllable Synthesis of 2D Nonlayered Cr_2S_3 Nanosheets and Their Electrocatalytic Activity Toward Oxygen Evolution Reaction. *Front. Chem. Eng.* **2021**, *3*, 1–7. [CrossRef]
49. Shamsipur, M.; Taherpour, A.; Sharghi, H.; Lippolis, V.; Pashabadi, A. A Low-Overpotential Nature-Inspired Molecular Chromium Water Oxidation Catalyst. *Electrochim. Acta* **2018**, *265*, 316–325. [CrossRef]
50. Craig, M.J.; García-Melchor, M. High-Throughput Screening and Rational Design to Drive Discovery in Molecular Water Oxidation Catalysis. *Cell Rep. Phys. Sci.* **2021**, *2*. [CrossRef]
51. Sun, Z.; Yuan, M.; Yang, H.; Lin, L.; Jiang, H.; Ge, S.; Li, H.; Sun, G.; Ma, S.; Yang, X. 3D Porous Amorphous γ-CrOOH on Ni Foam as Bifunctional Electrocatalyst for Overall Water Splitting. *Inorg. Chem.* **2019**, *58*, 4014–4018. [CrossRef]
52. Kumar, U.N.; Malek, A.; Rao, G.R.; Thomas, T. Chromium Oxynitride (CrON) Nanoparticles: An Unexplored Electrocatalyst for Oxygen Evolution Reaction. *Electrocatalysis* **2022**, *13*, 62–71. [CrossRef]